J Mater Sci (2008) 43:6473–6479
DOI 10.1007/s10853-008-2986-2

Preparation and phase development of yttria-doped ceria coated TZP powder

Darunee Wattanasiriwech · Suthee Wattanasiriwech

Received: 26 July 2008 / Accepted: 2 September 2008 / Published online: 17 September 2008
© Springer Science+Business Media, LLC 2008

Abstract This paper presents a simple technique for preparation of yttria-doped ceria (YDC) coated tetragonal zirconia polycrystal (3Y-TZP) powder and its phase development upon firing. The coating solution was prepared using yttrium nitrate hexahydrate and cerium nitrate hexahydrate as starting reagents. Thermochemical reactions of the coated powder were studied using TGA and FTIR while phase development upon firing was examined using XRD. Inward diffusion of the coating YDC into the TZP particles was monitored by observing the change of crystal structure and lattice parameter as a function of sintering temperature and time. At sintering temperature of 1300 °C for 1 h, crystal structure of the sample was still tetragonal (t-ZrO_2). Increasing sintering time to 5 h at 1300 °C, diffusion of YDC into TZP particles occurred drastically and the structure was changed to cubic (c-ZrO_2) as indicated by the disappearance of (002)/(200) peak splitting. Increasing sintering temperature to 1400 and 1500 °C, however, resulted in the co-existence of tetragonal and cubic phases as indicated by the appearance of triples around 72.5–74° 2θ and also the decrease of cubic lattice parameter. When the sintering temperature was further increased to 1600 °C, lattice parameter was only slightly changed, suggesting that inward diffusion of YDC reached saturation point around this temperature.

D. Wattanasiriwech (✉) · S. Wattanasiriwech
School of Science, Mah Fah Luang University,
Chiang Rai 57100, Thailand
e-mail: d.wattana@hotmail.com

Introduction

Cubic-stabilized zirconia (CSZ) has been used as an oxygen ion conducting solid electrolyte in high temperature (900–1000 °C) solid oxide fuel cell (SOFC) for a number of years. The major problem with the current model of the SOFCs is its capital cost. This cost is partly due to the high operating temperatures and thus the need for very expensive high temperature alloys in the system. An instant solution is to reduce the operating temperature to 500–700 °C so that conventional stainless steels can be used. To do this, a new type of electrolyte is required and the most promising one so far has been ceria-based materials. Ceria (CeO_2) has a fluorite structure and a lattice parameter of 5.41 Å [1]. Ceria doped with rare earth oxides such as La_2O_3, Y_2O_3, Sm_2O_3, and Gd_2O_3 was reported to have high ionic conductivity and may be used as a solid electrolyte in fuel cells [2–7]. According to Steele et al., the negative charge occurred in CeO_2 lattice due to the aliovalence substitutions were balanced by oxygen vacancies [8]. It had been reported that ceria-based materials such as gadolinia-doped ceria (GDC), yttria-doped ceria (YDC), or samaria-doped ceria (SDC), exhibited much higher ionic conductivity than CSZ at intermediate temperatures (~600 °C). Although ceria-based ceramics exhibited satisfactory electrical conductivity, their mechanical properties especially fracture toughness were relatively poor. Bending strength of the sintered GDC fabricated from precipitated powders was found to be 143 ± 10 MPa at room temperature and 115 ± 12 MPa at 800 °C [9]. Fracture toughness of this material was only 2.48 MPa $m^{1/2}$. Improvement of mechanical properties of this ceramic was important for fabrication and employment in SOFCs. An attempt to improve mechanical properties of ceria-based ceramic by addition of alumina was found to deteriorate its

electrical conductivity especially the grain boundary conductivity due to the formation of $GdAlO_3$ phase [10]. Interaction between GDC electrolyte and yttria-stabilized zirconia (YSZ) anode which gave rise to solid solution phases was also problematic to the effectiveness of the cell [11, 12]. This was because the solid solution phases exhibited lower ionic conductivity than either GDC or CSZ. Thus employment of ceria-based material in place of CSZ still needs further work to eliminate this problem.

Solution coating technique had been employed to improve properties of zirconia ceramics [13–15]. Improved grain boundary conductivity and thermal shock resistance of 2.9 mole% yttria-doped zirconia fabricated from a commercial yttria-coated zirconia powder was reported [13]. When this powder was compacted and sintered at 1300–1750 °C, a core-shell structure of monoclinic-tetragonal was obtained. Fabrication of Ce–TZP for the purpose of improved mechanical property by a solution coating technique was also reported although a detail study of phase development was not addressed [14, 15].

In this research, the authors intended to combine mechanical properties of TZP and electrical properties of YDC. TZP (2–3 mole% Y_2O_3) had been reported to exhibit excellent mechanical properties [16–19]. When it is coated with YDC and sintered, inward diffusion of YDC into the TZP powder should occur. Crystal structure of the coated TZP powder was controlled by changing the sintering condition. At a proper sintering condition, a core-shell structure could possibly be obtained.

Experiments

The mole ratio of the YDC coating solution to TZP powder used in this research was 1:10 and the composition of the coating was $Ce_{0.90}Y_{0.10}O_{1.95}$. The molar percentage of CeO_2 and Y_2O_3 presented in the ceramic was thus 8.2 and 3.2, respectively.

The TZP powder was commercial powder with 3 mole% yttria content and the specific surface area of 16 ± 3 m^2/g (TZ-3Y; TOSOH, Japan). Particle size of the powder was calculated from the specific surface area using the equation:

$$d = 6/\rho As \quad (1)$$

where As is the specific surface area (m^2/g), ρ (6.05 g/cm^3) is the density value of TZP provided by the supplier, and d is the particle diameter.

The coating solution was prepared as follows: first stoichiometric amounts of yttrium nitrate hexahydrate ($Y(NO_3)_3{\cdot}6H_2O$; Aldrich), cerium nitrate hexahydrate ($Ce(NO_3)_4{\cdot}6H_2O$; Aldrich) were dissolved in water at 80 °C. PVA ($(-CH_2CH(OH)-)_n$; average Mw 85,000–146,000; Aldrich) with the quantity equal to 1 wt.% of TZP powder was added to the solution to improve the green strength of the powder compact. When the starting reagents were completely dissolved, weighed amount of TZP powder was added. A small amount of Dispex (Ciba Specialty Chemicals, UK) was also incorporated to control the dispersion behavior of the slurry. The slurry was continuously stirred at a constant temperature of 80 °C on a hot plate until the solvent was completely evaporated. The resulting powder was then hand-ground and subsequently sieved through a 150-mesh sieve. FTIR spectroscopy technique (Perkin–Elmer Instruments, Spectrum GX, Germany) was employed to examine the different constituents between the as-coated powder and the powder calcined at 900 °C. Thermal analysis of the coated powder was determined in air using TGA/SDTA 851^e STAR^e thermobalance (Mettler Toledo, Switzerland). For powder compaction, the sieved powder was uniaxially pressed at 100 MPa and sintered in an electric furnace at 1300–1600 °C for 1–5 h in air. Phase changes of the sintered samples and crystal size of the coated powder were determined using XRD and X'pert Data Viewer software (PANalytical, X'pertPro MPD, the Netherlands). Calculation of crystal size was based on Scherrer's formula and full width at half maximum (FWHM) value. To extend the understanding of phase development upon firing, the coated powder was calcined from 300 to 1,100 °C for 1 h prior to XRD analysis. Microstructures of the as-coated powder and the as-sintered samples were examined using SEM (JEOL, JSM–5410LV, Japan).

Results and discussions

Basic studies of the starting powders

The SEM micrograph for the as-coated TZP powder is shown in Fig. 1. Particle size of the powder calculated from the surface area was in the range of 50–80 nm while it was around 50 nm when calculated from the XRD spectrum. The FTIR spectrum for the as-coated powder and the same powder calcined at 900°C are comparatively shown in Fig. 2. The $-CH_2-$, $-CH_3$, and –OH groups indicated in the spectrum belonged to the added PVA. The presence of $O-NO_2$ signals at 1616 and 1300 cm^{-1} in the as-dried powder confirmed that cerium nitrate and yttrium nitrate added to the TZP powder were still in the nitrate forms. The absence of $O-NO_2$ signals in the calcined powder indicated that cerium and yttrium nitrate had already changed to oxides below 900 °C. Thermal analysis result of the coated powder is shown in Fig. 3. TGA curve indicated two weight loss steps. The first step occurred from room temperature to approximately 120 °C with the

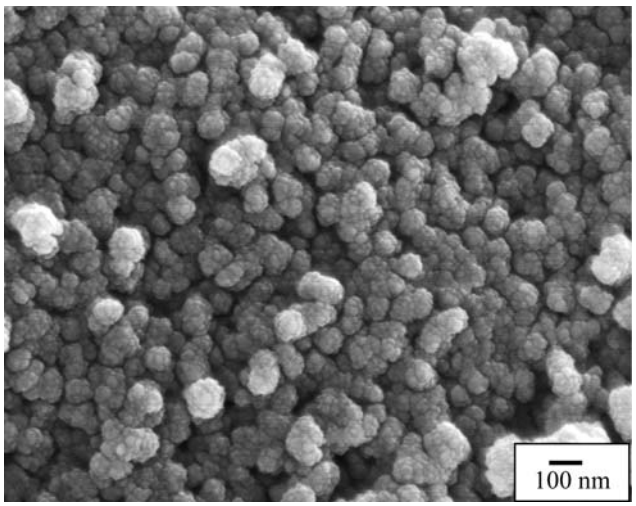

Fig. 1 SEM micrograph of the YDC-coated TZP powders

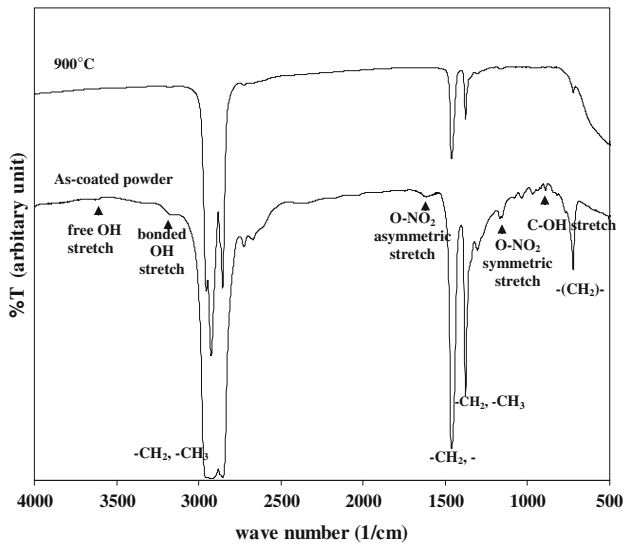

Fig. 2 FTIR spectrum for the dried and calcined YDC-coated TZP powders with the key functional groups labeled

weight loss of 4% and the second step occurred at ~250 °C with the weight loss of 7%. DTA result showed that both weight loss processes were endothermic with different mechanisms. The first process occurred gradually due to the loss of volatile components such as the crystallized water or the added organic compounds while the second process occurred abruptly due to the decomposition of nitrates into oxides. The endothermic signal which started around 1100 °C was probably due to the inward diffusion of the coating YDC into the host TZP powder. This explanation was confirmed with the XRD results in "Phase changes" section.

Phase changes

Coated powders

XRD results for the as-coated and the calcined powders are shown in Fig. 4. The as-coated powder was mainly tetragonal (t-ZrO_2) with a minor amount of monoclinic (m-ZrO_2) phase. The CeO_2 peaks started to appear after the powder was calcined at 300 °C for 1 h. When the calcination temperature was increased to 800–900 °C, the intensity of the CeO_2 peaks increased while those of m-ZrO_2 decreased and finally disappeared. Diffusion of CeO_2 into the host TZP grains could start at 1100 °C, as indicated by the decrease of CeO_2 peak intensity.

Compacted Powders

The XRD patterns of the representative samples are shown in Fig. 5. Since the starting powder was coated with YDC on the outer surface, distribution of YDC in the host TZP grains at the beginning was nonuniform. As it was well acknowledged, diffusion of an ion was a temperature and time dependent process, the changes of the crystal structure as a function of temperature and time was thus of our

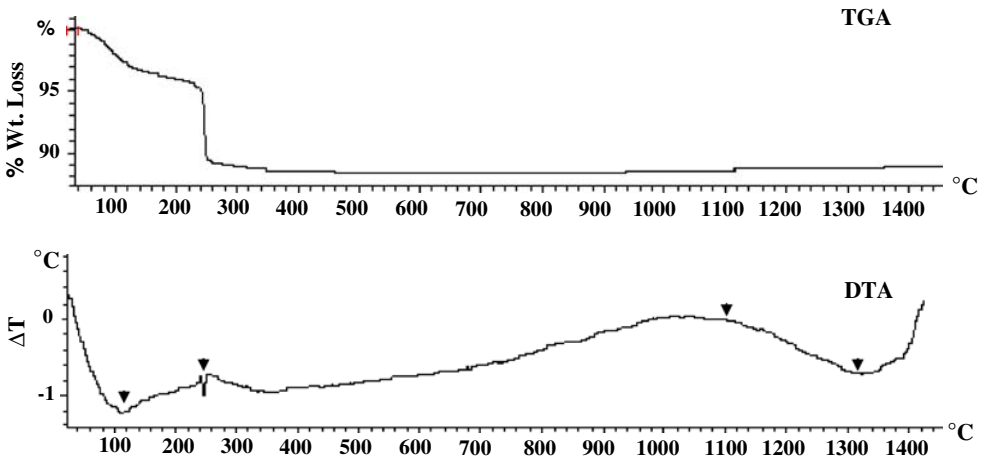

Fig. 3 TGA and DTA curves for the YDC-coated TZP powder. The arrows indicate the change of thermal energy due to chemical and physical reactions

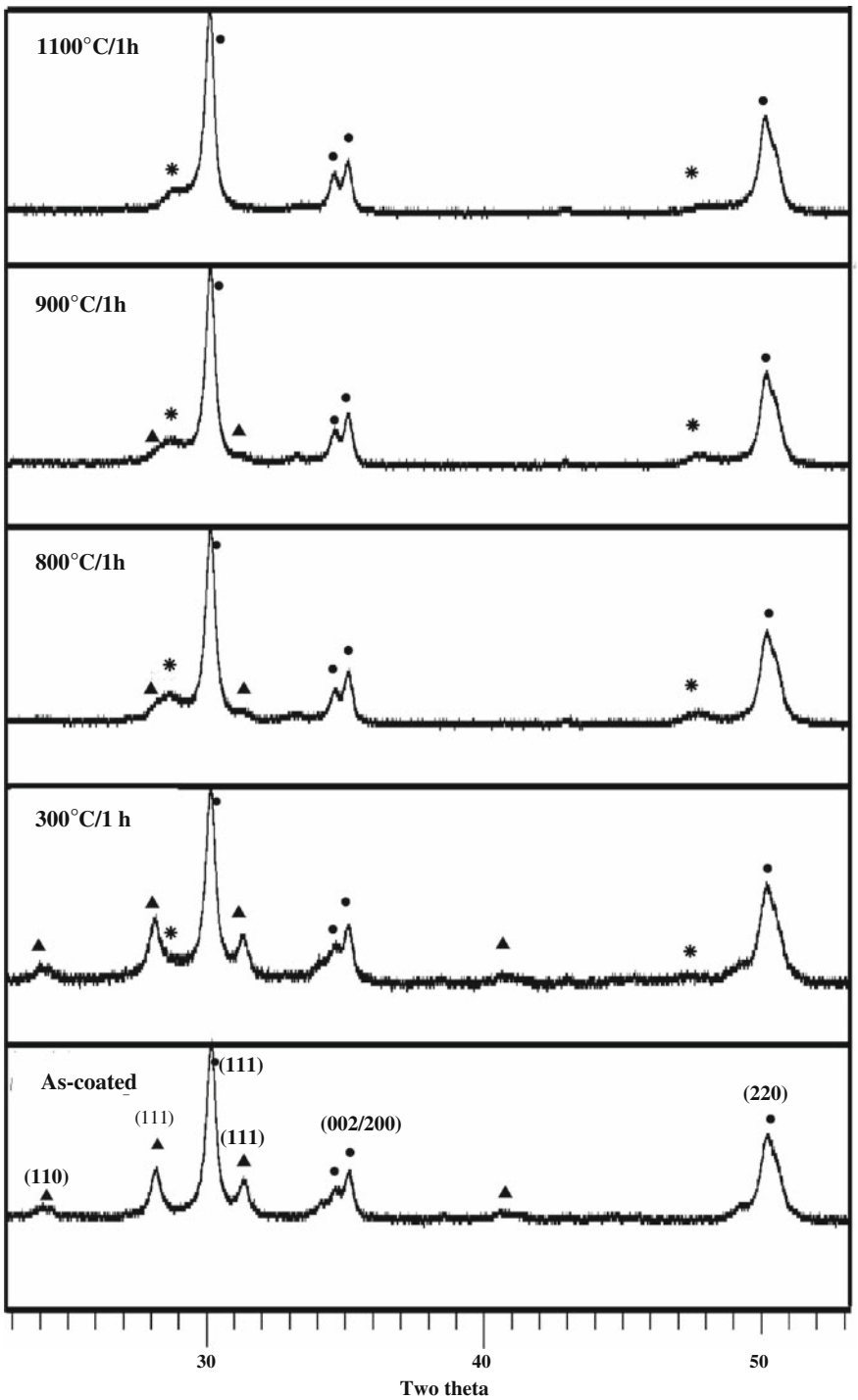

Fig. 4 XRD patterns for the as-coated powders and the coated powder calcined at different temperatures for 1 h. (●) t-ZrO_2, (▲) m-ZrO_2, (✳) CeO_2

interest. An ionic radius of Ce^{4+} is 0.92 nm while that of Y^{3+} is 1.014 nm [1]. When zirconium ion (ionic radii = 0.84 nm) is substituted by ions with larger ionic radii, structural change, lattice distortion, and XRD peak shift corresponding to the change of lattice parameters could occur. In this study, the changes of crystal structure and lattice parameters were observed as a function of sintering temperature and time. At the sintering condition of 1300 °C for 1 h, a trace of ceria was still observable and the sample was still in the tetragonal form as indicated by the (002)/(200) and (113)/(131) doublets. Increasing the sintering time to 5 h at 1300 °C resulted in the change from tetragonal to cubic structure as indicated by the change of the doublets into single peaks. Besides, the existence of ceria was no longer observed at this sintering condition. When the sintering temperature was further increased to

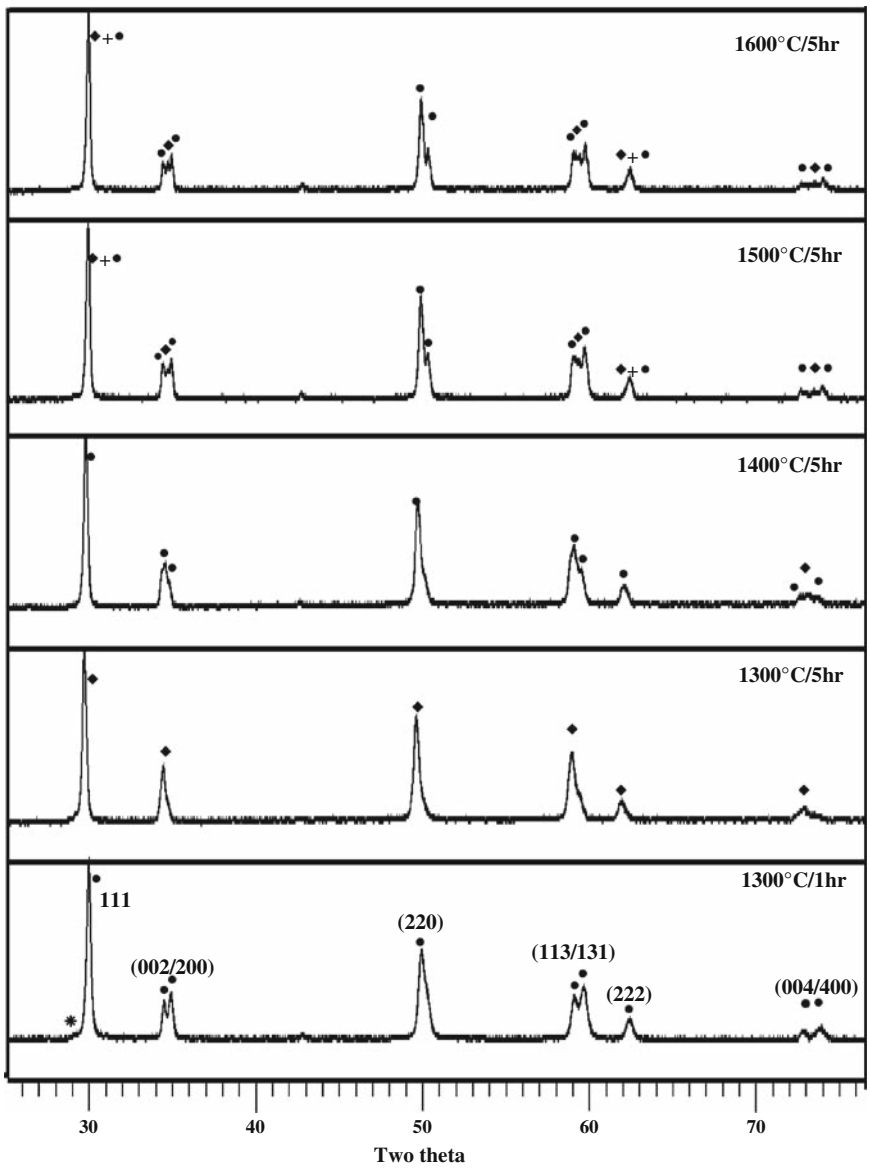

Fig. 5 XRD patterns for the compacted YDC-coated TZP powders sintered at different conditions. (●) t-ZrO_2, (◆) c-ZrO_2, (✳) CeO_2

1400 °C for 5 h, the crystal structure was changed from cubic to cubic + tetragonal which was characterized by the triplets around 72–74° 2θ. Increasing sintering temperature to 1500 and 1600 °C resulted in a more apparent cubic + tetragonal character as suggested by the appearance of other triplets around 34° 2θ. A similar phase change from tetragonal to cubic and then to cubic + tetragonal structures was also observed in the samples sintered from 1300–1600 °C for 3 h.

Additional to the phase change, the shift of cubic peaks towards higher values of 2θ was also observed when the sintering temperature was increased from 1300 to 1600 °C for 5 h. Therefore, lattice parameters of the cubic phase were calculated from the whole spectrum following the method described by Cullity [20] and plotted as a function of sintering condition, as shown in Fig. 6. It is noted that

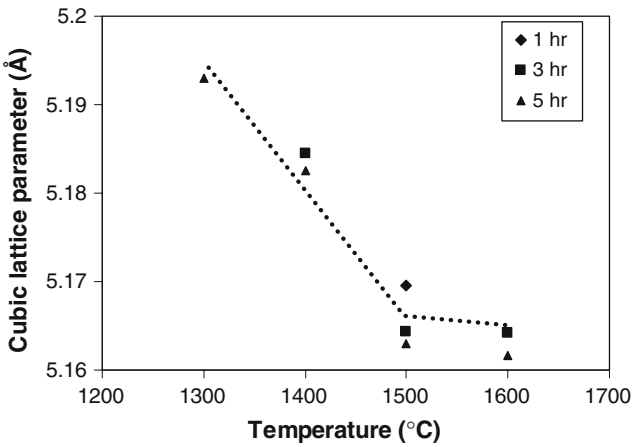

Fig. 6 Changes of cubic lattice parameters of the compacted zirconia powder as a function of sintering temperature and time

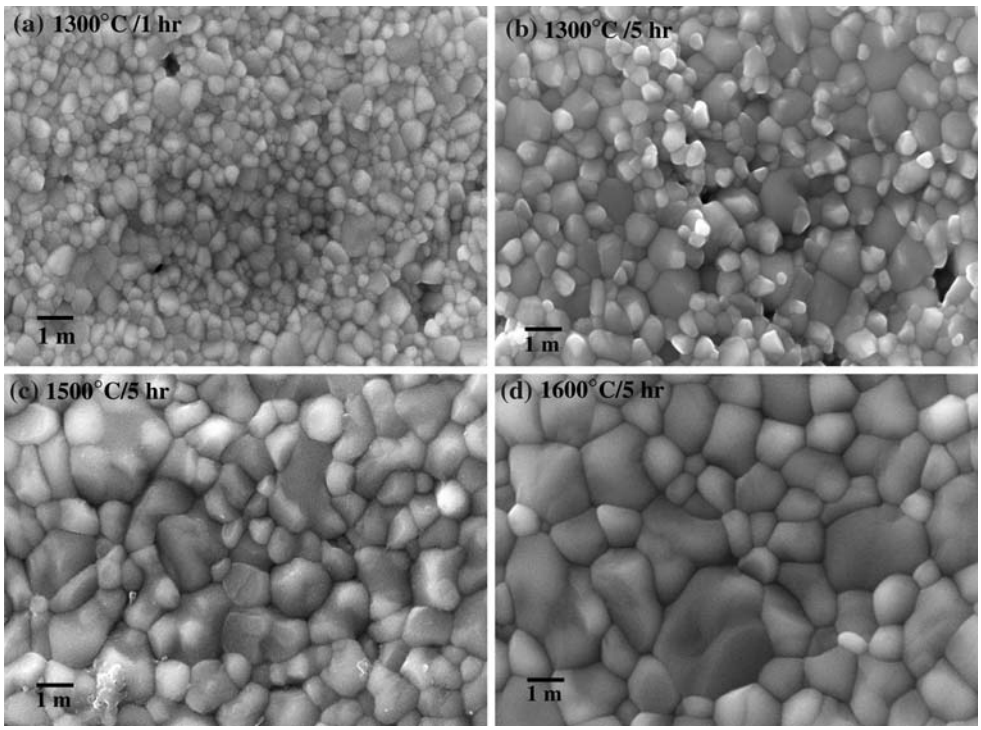

Fig. 7 SEM micrographs showing the effect of sintering conditions on microstructure development of samples sintered at (**a**) 1300 °C for 1 h, (**b**) 1300 °C for 5 h, (**c**) 1500 °C for 5 h, and (**d**) 1600 °C for 5 h

some sintering conditions in which the cubic phase did not exist were not included in the plot. When the sintering temperature was increased from 1300 to 1500 °C, the cubic lattice parameter was dramatically decreased. Further increasing the sintering temperature to 1600 °C, the lattice parameter was only slightly changed. In YSZ, the decrease of cubic lattice parameter corresponded to the decrease of yttrium content [21–24]. It was thus believed that a decrease of cubic lattice parameter with an increase of sintering temperature observed in this work was due to the progressive inward diffusion of the Ce^{4+} and Y^{3+} stabilizers from the outer rim of the grains into the core.

From the XRD results, diffusion of YDC into TZP could probably be divided into three stages. At stage I (~1300 °C for 1 h), diffusion was only slightly, so tetragonal phase was still observed. At stage II (~1300 °C for 5 h), drastic diffusion could occur on the outer rim and the structure was changed to cubic. At the final stage (~1400 °C and above), thoroughly diffusion had occurred and the co-existence of tetragonal and cubic phases was detected.

Microstructure

SEM micrographs in Fig. 7 show the dependence of microstructure on sintering condition for the YDC-coated TZP compact powder. The samples sintered at 1300 °C for 1 h exhibited typical characteristic of TZP ceramics, i.e., uniform grains with submicron in size (Fig. 7a). The XRD analysis result had confirmed that the major phase of this sample was tetragonal. Although small amount of CeO_2 could be detected by XRD in the samples sintered at this condition, it could not be observed in the SEM micrograph. When the sintering time was extended to 5 h, the proportion of larger grains with more than 1 μm in size significantly increased (Fig. 7b), associated with the existence of the cubic phase in the XRD spectrum. Complete densification and further grain growth were observed in the samples sintered at 1500–1600 °C as shown in Fig. 7c and d, of which the XRD results revealed the coexistence of tetragonal-cubic phases.

Conclusion

YDC-coated TZP had been prepared by a solution coating technique in which the YDC nitrates were coated onto the TZP powder by a simple mixing method. The coating YDC nitrates had crystallized into oxides around 250 °C. Inward diffusion of YDC into the host TZP particles possibly started around 1100 °C as suggested by both DTA and XRD results. In the sample sintered at 1300 °C for 1 h, partially diffusion of YDC coating occurred and the observed structure was tetragonal. When the coated sample was isothermally sintered for 5 h, the detected structure had become cubic which was believed to be due to extensive diffusion of YDC into the outer rim of TZP grains. When the sintering temperature was further increased to 1400–1600 °C, the XRD results displayed the coexistence of tetragonal and cubic phases as well as the

decrease of cubic lattice parameters. Such temperatures probably promoted further diffusion and resulted in a uniform distribution of dopant within the matrix of zirconia.

References

1. Mogensen M, Sammes NM, Tompsett GA (2000) Solid State Ion 129:63. doi:10.1016/S0167-2738(99)00318-5
2. Kudo T, Obayashi HJ (1975) Electrochem Soc 122(1):142. doi:10.1149/1.2134143
3. Hatchewell C, Sammes NM, Brown IWM (1999) Solid State Ion 126:201. doi:10.1016/S0167-2738(99)00232-5
4. Pérez-Coll D, Nùñez P, Frade JR, Abrantes JCC (2003) Electrochim Acta 48:1551. doi:10.1016/S0013-4686(03)00027-6
5. Balazs GB, Glass RS (1995) Solid State Ion 76:155. doi:10.1016/0167-2738(94)00242-K
6. Inaba H, Tagawa H (1996) Solid State Ion 83:1. doi:10.1016/0167-2738(95)00229-4
7. Steele BCH (2000) Solid State Ion 129:95. doi:10.1016/S0167-2738(99)00319-7
8. Steele BCH, Floyd JM (1971) Proc Br Ceram Soc 19:55
9. O-Bellon NM, Sammes J, Staniforth S (1998) J Powder Sour 75:116. doi:10.1016/S0378-7753(98)00104-9
10. Zhang T, Zeng Z, Huang H, Hing P, Kilner J (2002) Mater Lett 57:124. doi:10.1016/S0167-577X(02)00717-6
11. Zhou XD, Scarfino B, Anderson HU (2004) Solid State Ion 175:19. doi:10.1016/j.ssi.2004.09.040
12. Tsoga A, Gupta A, Naoumidis A, Nikolopoulos P (2000) Acta Mater 48:4709. doi:10.1016/S1359-6454(00)00261-5
13. Bowen CR, Tavernor AW, Luo J, Stevens R (1999) J Eur Ceram Soc 19:149. doi:10.1016/S0955-2219(98)00198-8
14. Huang SG, Li L, Van der Biest O, Vleugels J (2007) J Eur Ceram Soc 27:689–693. doi:10.1016/j.jeurceramsoc.2006.04.040
15. Yuan ZX, Vleugels J, Van Der Biest O (2000) Mater Lett 46(5):249–254. doi:10.1016/S0167-577X(00)00180-4
16. Gupta TK, Lange FF, Bechtold JH (1978) J Mater Sci 13:1464. doi:10.1007/BF00553200
17. Amin KE, Nag D (1995) Am Ceram Soc Bull 74(5):80
18. Lee SW, Hsu SM, Shen MC (1993) J Am Ceram Soc 76(8):1937. doi:10.1111/j.1151-2916.1993.tb08315.x
19. Dauskardt RH, Yu W, Ritchie RO (1987) J Am Ceram Soc 70(10):C-248. doi:10.1111/j.1151-2916.1987.tb04889.x
20. Cullity BD (1978) Elements of X-ray diffraction, 2nd edn. Addison-Wesley Publishing Company, Inc, pp 327–330
21. Howard CJ, Hill RJ, Reichert BE (1995) Appl Crystallogr 28:206. ICSD collection code 062994; zirconium yttrium oxide ($(Zr_{0\cdot935}Y_{0.065})O_{1.968}$)
22. Yashima M, Sasaki S, Sakihana M, Yamaguchi Y, Arashi H, Yoshimura M (1994) Acta Crystallogr Sec B. Struct Sci 50:663. ICSD collection code 075316; zirconium yttrium oxide ($Zr_{0\cdot8}Y_{0.2}O_{1.9}$)
23. Morinaga M, Cohen JB (1979) Acta Crystallogr Sec A 35:745, 975. ICSD collection code 060605; zirconium yttrium oxide ($(Zr_{0\cdot786}Y_{0.214})O_{1.7}$)
24. Ingel RP, Lewis D (1986) J Am Ceram Soc 69(4):325. doi:10.1111/j.1151-2916.1986.tb04741.x